

Charging of Ligand-Protected Gold Nanoparticles in Electrospray Ionization: Probing Ligand Bond Strength by Charge Detection Mass Spectrometry

B. S. Sooraj, Sylvain Maclot, Anagha Jose, Clothilde Comby-Zerbino, Tessa Reinert, Keerthana Unni, Rodolphe Antoine,* and Thalappil Pradeep*



Cite This: *J. Phys. Chem. Lett.* 2025, 16, 7004–7011



Read Online

ACCESS |



Metrics & More

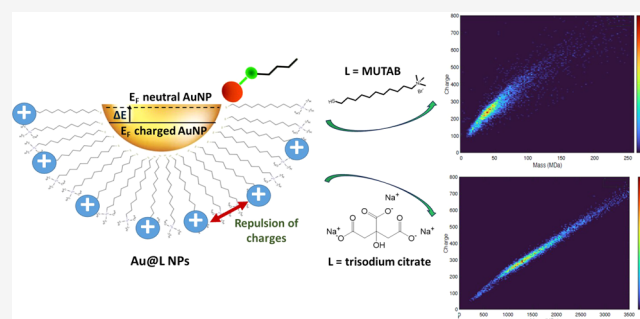


Article Recommendations



Supporting Information

ABSTRACT: The ionization of large, megadalton (MDa) and gigadalton (GDa), nanoparticles leading to their mass spectrometric analysis has been an interesting challenge in the past decades. In this work, the charging behavior of 20 nm sized gold nanoparticles (AuNPs) protected with 11-mercaptoundecyl-*N,N,N*-trimethylammonium bromide (MUTAB) ligands of ~50 MDa was studied by using Charge Detection Mass Spectrometry (CDMS) interfaced with electrospray ionization. The findings indicate that these nanoparticles can achieve a charging state higher than the Rayleigh limit for a 20 nm solvent droplet. However, citrate-protected 60 nm sized AuNPs of ~1.3 GDa charge only ~0.45 times the Rayleigh limit, under identical electrospray conditions. The higher efficiency of charging in Au–MUTAB nanoparticles may be correlated to the higher ligand binding energy of the gold–sulfur interface compared to the gold–citrate interface. This work showcases the impact of ligand selection on the electrostatic behavior, stability, and charging of nanoparticles in electrospray ionization mass spectrometric applications.



Ligand-protected metal nanoparticles are a class of materials well-known for their diverse applications.^{1–7} Understanding the composition of these materials is crucial for tuning their properties.⁸ However, nanoparticles have an intrinsic size dispersion leading to high heterogeneity in both mass and charge, which prevents their analysis by conventional mass spectrometry techniques.⁹ Indeed, as heterogeneity is very high, resulting *m/z* spectra are highly congested and do not provide useful information.¹⁰ Single-ion MS methods¹¹ overcome these limitations by directly measuring the mass for each individual ion. In the past decade, charge detection mass spectrometry (CDMS), a single-ion MS method, has evolved as an alternative technique for weighing heterogeneous samples¹² with masses in the megadalton (MDa) range.¹³ CDMS (and related orbitrap-based CDMS) combines mass spectrometry (MS) with (direct or indirect) charge detection to measure the charge and *m/z* ratio of individual particles.^{14,15} Further, all the individual nanoparticle measurements are compiled into histograms to obtain the charge and mass distribution of the sample.¹⁶ Werts et al. first demonstrated the importance of CDMS in a low mass resolution mode for the determination of the size distribution and composition of gold nanoparticles, where the mass can be directly translated to particle size, if the density and shape of the particle are known.¹⁷ Advancements in CDMS instrumentation further demonstrated its application in characterizing assemblies of

larger nanoparticles, providing insights into their shape, surface properties, etc.^{18–20}

In the past, charging of nanoparticles through electrospray ionization (ESI) has been a topic of significant interest.^{21,22} In ESI, highly charged droplets are generated from solutions, followed by solvent evaporation and droplet fission, leading to particles (or analytes) carrying multiple charges.²³ In ESI, the maximum charge a liquid droplet could accommodate without undergoing Coulombic fission is driven by the Rayleigh limit.²⁴ This limit originates from the competition between the bulk electrostatic repulsion and the interfacial surface tension. Beyond this limit, the droplet becomes unstable and splits into smaller droplets with lower charges. The Rayleigh limit serves as a benchmark for assessing the charging capacity of charged analytes transferred into the gas phase by the electrospray process.²⁵ The charging phenomenon is dependent on various factors, such as the size and shape of the analyte and instrumental settings, etc. In the past decade, several studies

Received: April 9, 2025

Revised: June 24, 2025

Accepted: June 26, 2025

Published: June 30, 2025



were reported on increasing charging of analytes in ESI. The commonly used strategies include, changing solvent composition, pH, addition of supercharging agents, etc.^{26,27} However, for nanoparticles, these strategies were limited to polymeric nanoparticles²¹ and such efforts were not very successful in achieving high charging for ligand-protected metal nanoparticles.

In this work, we utilize ligand engineering as a strategy to achieve a high charging capability of gold nanoparticles. The limit of charge detection has drastically improved from ~ 350 e (elementary charges) in the first generation of CDMS instrument²⁸ to ~ 70 e in the present CDMS instrument which uses cool field-effect transistor (coolFET) based detection.²⁹ Here, we have performed the CDMS analysis of a 20 nm sized gold nanoparticle protected with a cationic thiol ligand, i.e., (11-mercaptoundecyl)-*N,N,N*-trimethylammonium bromide (MUTAB). These results were compared with that of a 60 nm citrate-protected Au nanoparticle to demonstrate the role of the MUTAB ligand in the charging. The MUTAB ligand provides electrostatic stabilization and enhances the charge-carrying capacity of the nanoparticles, boosting the charging capabilities of the NPs. The higher efficiency of MUTAB in enhancing nanoparticle charging may be correlated to the strength of the thiol-gold binding (leaving the ammonium group free), which is stronger than gold-citrate interaction. A simple model is derived to evaluate the ligand binding strength of gold nanoparticles by charge and mass (or size) measurements through CDMS.

The 20 nm sized Au–MUTAB nanoparticles were synthesized using a reported procedure.³⁰ The size distribution of the nanoparticle was studied by transmission electron microscopy (TEM), and the images were collected at a lower beam intensity to reduce beam-induced aggregation, as shown in Figure 1c. The images showed that the Au–MUTAB nanoparticles are spherical in shape. The diameter distribution of the particles ranged from 10 to 30 nm, where most of the particles were close to 20 nm in diameter. These nanoparticles were subjected to CDMS analysis, and we obtained a spectrum

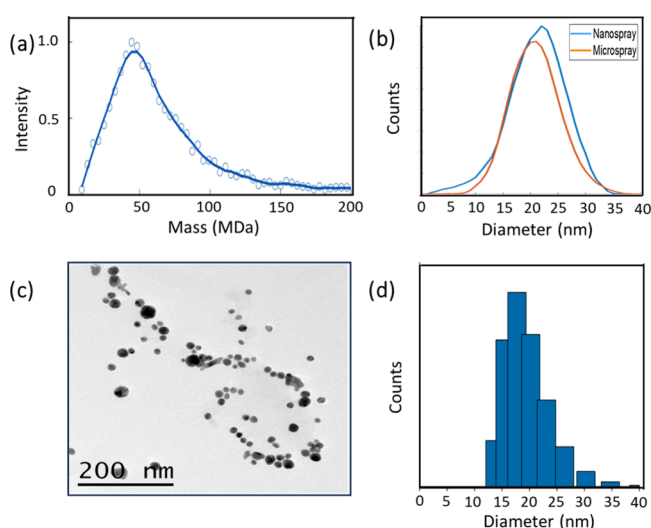


Figure 1. (a) Mass distribution of Au–MUTAB nanoparticles obtained from CDMS analysis; (b) size distribution estimated from the CDMS data obtained under two different spray conditions; (c) TEM image of Au–MUTAB nanoparticles; and (d) size distribution of Au–MUTAB nanoparticles obtained from DLS measurements.

(Figure 1a) showing the peak maximum at 50 MDa. We have translated the mass obtained from CDMS to the size of the particle by considering their density and shape. The obtained size from these calculations was 20 nm, which corresponds to the mass of 50 MDa for a spherical gold particle with a density of 19.3 g/cm^3 (Figure 1b). This was further verified by using dynamic light scattering (DLS) measurements, as shown in Figure 1d. The measurements were performed using water as the solvent medium. The size distribution showed a similar size range of 10 to 30 nm, which showed a maximum at 20 nm.

The CDMS analysis of the Au–MUTAB nanoparticles was conducted under two different ionization conditions, i.e., nanospray and macrospray. Both of these techniques primarily differ in terms of the scale of the spray, the ionization technique, and the sample volumes that they handle. The samples used for the measurements were diluted in a water/methanol (1:1) mixture to a concentration of $50 \mu\text{M}$ (in terms of elemental gold concentration). Figure S1 shows the data obtained from the CDMS analysis under both spray conditions. Figure S1a shows the mass versus charge data obtained for the sample under nanospray ionization conditions. Each point in the graph represents the measurement of a single ion. The streak extends from 100 e (elementary charges) to around 450 e. Figure S1b shows the typical mass distribution from CDMS, with a broad peak centered at 50 MDa. Figure S1c shows the charge distribution for each ion observed in the analysis, which shows a broad peak centered around 250 e due to the main peak of 50 MDa in mass distribution. The broad distribution in the mass distribution accounts to the polydispersity in the sample which is evident from their TEM and DLS measurements. The mass versus charge data obtained for the sample under macrospray ionization conditions are shown in Figure S1d. Here the streak extends from 100 e to around 500 e. Figure S1e shows a similar mass distribution, with a broad peak centered at 50 MDa that is more intense than the nanospray results. Figure S1f shows the charge distribution having a more intense peak centered at around 250 e only.

The data obtained from both nanospray and macrospray conditions were compared, as shown in Figure S2, to better understand the data. The mass distribution plot (Figure S2a) illustrates that in both cases the peaks are centered at 50 MDa. But for macrospray, the intensity of the peak at 50 MDa is more than in nanospray. This hints that, in macrospray, the analyzed sample has a greater number of species with 50 MDa mass, which can be due to the larger volume of the sample used. In the case of nanospray, we can observe more intense peaks in the higher mass region above 100 MDa. This slight increase in the intensity might be due to the formation of aggregated dimers. The particle size estimation from CDMS also shows similar results in both spray conditions (Figure S2b), which further supports the precision of our results.

The maximum charge deposited on a spherical ion can be predicted from the Rayleigh charge limit for a water droplet with the same diameter as the analyte. The charge corresponding to the Rayleigh limit, Z_R , is given by $eZ_R = 8\pi(\epsilon_0\gamma R^3)^{1/2}$ where R is the droplet radius, γ is the surface tension of droplets (72 nN/m), and ϵ_0 is the permittivity of the surrounding media.³¹ The theoretically calculated Rayleigh limit is illustrated in Figure 2a, where the dotted line indicates the limiting charge at the corresponding size distribution. To further understand this, we plotted the histogram of the fraction of the Rayleigh limit in the sample (Figure 2b). The

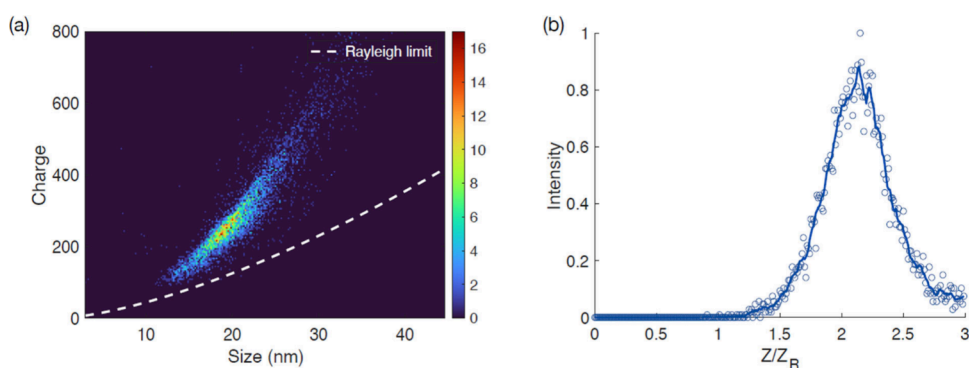


Figure 2. (a) Charge vs size plot of Au–MUTAB nanoparticles. The dotted curve shows the calculated Rayleigh limit. (b) Plots of the fraction of the Rayleigh limit (z/z_R) for Au–MUTAB nanoparticles.

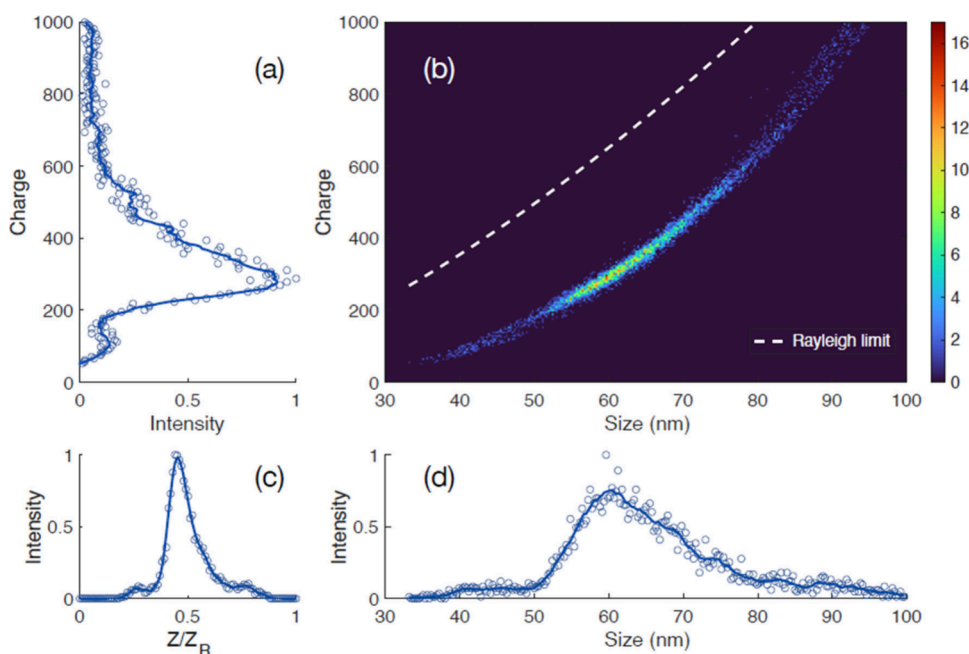


Figure 3. CDMS plots of a 60 nm sized Au–citrate nanoparticles showing the (a) charge distribution, (b) charge vs size plot, and (d) size distribution. The dotted curve in panel (b) shows the Rayleigh limit. (c) Plots of the fraction of the Rayleigh limit (z/z_R) for Au–citrate nanoparticles.

histogram shows that Z/Z_R ratio is centered around 2.1. It was already observed that ions from nanoparticles in the megadalton range were charged higher than the Rayleigh limit,^{18,32} demonstrating that the charging capability of nanoparticles cannot be necessarily driven by the charging of a water droplet with the same diameter as the analyte, which makes sense since nanoparticles may have different morphology, charging nature and origin as water droplets (they can be coated by ligands with permanent charges as it is the case in this study). The fact that MUTAB-capped AuNPs (20 nm size) have charging exceeding the Rayleigh limit means that the charging of electrosprayed NPs is not driven by the charging of a water droplet with the same diameter as the analyte. The charging capability is, in fact, driven by the stability of capping ligands on the NP surface, possessing permanent charges.

To understand the role of MUTAB ligands on the charging behavior of nanoparticles, we have also studied 60 nm sized gold nanoparticles protected with a citrate ligand. The size distribution of the particles obtained from TEM is shown in Figure S3. The size of the particles ranged from 40 to 80 nm,

and centered at 60 nm. The data obtained from the CDMS analysis of 60 nm sized Au–citrate nanoparticles are shown in Figure 3. The mass distribution shows a broad peak ranging from 700 to 2500 MDa, centered around 1300 MDa (Figure S4). The corresponding charge analysis shows a peak centered at 300e, with a broad distribution from 200 to 600e (Figure 3a). The charging capacity of the Au–citrate nanoparticle was compared with the Rayleigh limit of a 60 nm sized 1:1 water: methanol droplet, as illustrated in Figure 3b. The dotted lines imply that the charging capacity of the nanoparticle is much less than the limiting charges. A histogram of the fraction of Rayleigh limit in the sample was plotted (Figure 3c), which inferred that the Z/Z_R is centered around 0.45, with the maximum charge reaching ~ 70 – 80% of that corresponding to the Rayleigh limit, confirming their low charging capacity.

The spray conditions under negative ion mode using the standard pressurized electrospray inlet were much more difficult to reproduce and maintain than those under positive ion mode. Hence, the charging studies for both gold nanoparticles (AuNPs) were done in the positive ion mode.

Table 1. Summary of the Findings for Citrate-Capped and MUTAB-Capped Gold Nanoparticles by CDMS and DLS Analysis, Leading to the Estimation of the Binding Energy, E_{L-Au}

Type of nanoparticles	Z	R (nm)	N	U (eV)	E_{L-Au} (eV) Present work	E_{L-Au} (eV) Literature
MUTAB- capped gold nanoparticles	250	10	6280	6590	1.05	1.7 (Au-S) ³³
Citrate-capped gold nanoparticles	270	19	6280–35343 ^a	2907	0.06–0.36 ^a	0.09 (Au-O _{COOH}) ³⁴
	297	25	8050–47300 ^a	3200	0.09–0.51 ^a	
	358	35	12315–69272 ^a	3290	0.05–0.27 ^a	

^aThe range of E_{L-Au} is due to the uncertainty in estimating “N”, which in turn is due to the uncertainty in estimating the area per ligand.

Our results confirm that the MUTAB ligand plays a crucial role in increasing the charge-carrying capacity of the ligand-protected AuNPs. The long alkyl chain of MUTAB contributes to steric stabilization, preventing nanoparticle aggregation and maintaining colloidal stability even under high-charge conditions. However, the citrate-capped AuNPs only achieve charge states much lower than the Rayleigh limit due to limited surface charge density and weaker electrostatic stabilization. Hence, the nature of the protecting ligand is crucial in developing methodologies for charging a nanoparticle under electrospray ionization. To understand whether there is a role for the negative charge of citrate ligands in the lower charging behavior of Au–citrate nanoparticles, we analyzed different sizes of citrate-capped AuNPs with 40, 60, and 80 nm diameters. The size distribution of these particles obtained from DLS measurements is shown in Figure S5. The charge and mass data obtained from CDMS are shown in Figure S6. The average charge increases from 270e to 297e to 358e for 40, 60, and 80 nm diameter particles, respectively. For 80 nm AuNPs, we succeeded in measuring the ESI-CDMS in both positive and negative ionization modes (Figure S7). However, in negative mode, we observed that the particles appear to carry slightly higher charges than in positive mode (Figure S7e,f). The reason for this difference is that in the negative ionization mode, the source is prone to discharges, and it leads to two effects: (i) ion efficiency in ESI negative mode was severely reduced (by at least 1 order of magnitude), and (ii) unstable spray conditions may lead to incomplete desolvation and/or fragmentation (leading to broader mass and charge distribution). To better understand this, we have made a 2D plot of charge vs mass distribution for 80 nm AuNPs in both modes (Figure S7a,b). While comparing the charging for the same mass (expected for 80 nm AuNPs, e.g., ~3.11 GDa), we find that the charges are similar in both positive and negative modes of ionization. Hence, the charge distributions in both modes are similar, suggesting that charging capability is not driven by the charge state of the ligands in nanoparticles.

To better appreciate this issue, we aim to develop a simple model to link the charging capability of ligand-protected gold NPs with energetic considerations and particularly the ligand-gold binding properties. Let us assume that citrate- and MUTAB-capped gold nanoparticles are uniformly charged spheres. In these nanoparticles, we have a distribution of charges specified by a charge density, $\rho = Q/V$ (with $Q = Ze$ total charge and V is the volume of the sphere of radius R) and corresponding total electrostatic energy (where the sum of the energies of all possible pairs of charges to be replaced by an integral).

The total energy of a particle, expressed in terms of the total charge of the sphere is

$$U = \frac{3}{5} \frac{Q^2}{4\pi\epsilon_0 R} \quad (1)$$

The isopotential (R, Z) map of the electrostatic energy U (in eV) for a nanoparticle of charge Z and radius R is given in Figure S8.

In 1882, Lord Rayleigh theoretically estimated the maximum charge Q_R a liquid droplet could carry; it is known as the Rayleigh limit, above which a charged, incompressible spherical droplet of radius R and surface tension γ becomes unstable:

$$Q_R = 8\pi\sqrt{\epsilon_0\gamma R^3} \quad (2)$$

This criterion was particularly powerful to model electrospray processes (e.g., charged residue model (CRM) where Rayleigh-charged nanodroplets that contain a single analyte evaporate to dryness). In particular, the observed agreement between the charges on the proteins and the charges on water droplets of the same size at the Rayleigh limit was attributed because of the multiply charged proteins being formed by CRM.

Let us assume now that for citrate- and MUTAB-protected gold nanoparticles, the limiting factor to charge them by electrospray process is given by the balance between the Coulomb repulsion energy (U) and the Ligand binding energy (E_{lb}) of the capping ligands to the gold surface, assuming that the charges reside on the ligands. Then the limit for charging will be given by

$$U = E_{lb} \quad (3)$$

The total ligand binding energy (E_{lb}) is a product of the number of ligands (N) and the binding energy of each ligand bound to the gold surface (E_{L-Au}), such that $E_{lb} = N \times E_{L-Au}$. By knowing the values of N, R , and Q , it is possible to estimate the binding energy E_{L-Au} as

$$E_{L-Au} = \frac{3}{5} \frac{Q^2}{4\pi\epsilon_0 RN} \quad (4)$$

The values of Z and R are estimated from the present CDMS analysis and DLS measurements, respectively. The value of N is calculated knowing the surface coverage of ligands (~5/nm² for thiolates³⁵ and 0.8–4.5/nm² for citrate^{36–38}) on the sphere. The estimated E_{L-Au} energies from the CDMS analysis (see Table 1) are in fair agreement with binding energies reported in the literature for thiolates and citrates. One can argue that the charging capability of gas-phase monolayer-protected metal particles generated by electrospray is driven by the binding energy of ligands, and therefore, charge detection mass spectrometry might be a pertinent probe of the ligand binding strength. The assumption here is that the ligands desorb as integrated units (-SR for MUTAB), although other bond dissociations can also occur. This channel (-SR loss) is most common in nanoparticles, although they dimerize to form RS-SR, R-S-R, and other units during thermal desorption.

Usually, in most modeling studies, the ligands are modeled as enveloping uniformly the surface of nanoparticles, assumed as a perfect sphere.³⁶ In our crude electrostatic model, we assume that MUTAB- and citrate-capped gold nanoparticles are uniformly charged spheres. The energy of such an arrangement can be calculated using classical electrostatics and is shown in eq 1. The effective charge of a nanoparticle can be deduced from zeta-potential measurements.²² The data obtained from zeta-potential and size measurements of all of the nanoparticles are presented in Table S1. With zeta potentials of 17.6 and -35 mV, the total charge in solution is respectively 20e and 112e for 20 nm MUTAB–AuNPs and 60 nm citrate–AuNPs. However, the charging capacity extracted by zeta measurements cannot be directly compared with gas-phase measurements since zeta potential is the potential difference between the surface of a solid particle and the surrounding liquid in which the particles are dispersed.

The ionization energy of a neutral metallic NP in a vacuum is higher than the corresponding work function of the bulk metal. Hence, electrons in neutral metallic NPs are at a Fermi level lower than that in the bulk metal. In a vacuum, the ionization energy of a neutral AuNP lies somewhere between that of a gold atom, 9.2 eV, and the work function of bulk gold metal, which is approximately 5.3 eV. When the NP is charged due to the presence of adsorbed ionic species or ligands, the difference between these ionization energies under neutral and charged conditions is related to the excess charge on the NP. The excess charge in the nanoparticle is directly related to the outer potential. Hence, when citrate molecules adsorb onto the AuNP, the surface potential of the AuNP changes, leading to the alteration of local Fermi energy levels of the metal nanoparticle, as was modeled by Girault and coworkers.³⁹ For instance, a surface atom carrying a nucleophilic molecule acquires a small positive charge, and the interior of the colloidal particles receives a corresponding negative charge. The Fermi potential at equilibrium is shifted to a more negative value.⁴⁰ Therefore, the charging energy is related to the Fermi energy. However, in our crude electrostatic model, we simplified the gold NP as a uniformly charged sphere, and the charge of the sphere is given by the number of ligands with permanent charges. A schematic representation of these concepts and correlations regarding ligand bond strength (brought by the gold–sulfur interface), charging energy (brought by the repulsion of charged ligands), and modification of the Fermi level of a gold NP due to chemisorption of thiolated ligands is shown in Scheme S1.

The composition of the highly charged Au–MUTAB nanoparticles was tentatively assigned using details in the literature on the surface coverage of ligands on a gold surface. The number of MUTAB ligands on a 20 nm sized spherical particle is estimated to be 6280, and the corresponding number of Au atoms was calculated as 246000, for a 50 MDa particle. The obtained composition of Au_{~246000}L_{~6280} was further verified by elemental analysis, using high-resolution scanning electron microscopy (HRSEM) coupled with energy dispersive X-ray spectroscopy (EDS), as shown in Figure S9. The ratio of the number percentages of Au and S atoms is in good agreement with the assigned composition. Dass et al. had previously reported a methodology to estimate the number of metal atoms and ligands using mathematical modeling, which is termed as the nanoscaling law.⁴¹ These reports show that for nanoparticles protected with linear chain alkyl thiol ligand, the number of Au atoms (N) and ligands (L) follows a

mathematical relation, $L = 1.82N^{2/3}$. The 2/3 scaling reflects the surface area to volume ratio of the Platonic solids.^{42,43} This suggests that as the size of the nanomolecule increases, the surface area to volume ratio decreases proportionally to the power of 2/3. This is because the volume scales with the cube of the linear size, while the surface area scales with the square. A log–log plot of the number of ligands vs gold atoms in linear alkyl chain thiol-protected gold nanoparticles is shown in Figure 4. Here, we have compared the tentatively assigned

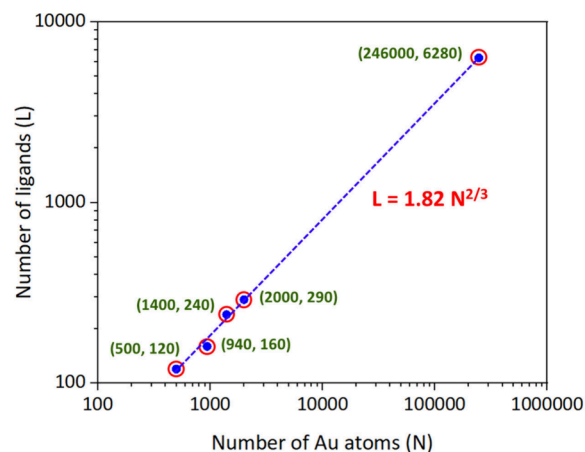


Figure 4. Log–log plot of the number of ligands vs gold atoms in linear alkyl chain thiol-protected gold nanoparticles (Au_{*n*}L_{*m*}). The composition (*m*, *n*) of previously reported nanoparticles is compared with the tentatively assigned composition of Au–MUTAB nanoparticles (246000, 6280).

composition of Au–MUTAB nanoparticles with some known nanoparticles. The larger-sized nanoparticles whose composition is determined to date are Au_{~2000}L_{~290},⁴⁴ Au_{~1400}L_{~240},⁴⁵ Au_{~940}L_{~160},⁴⁶ and Au_{~500}L_{~120}.⁴⁷ Figure 4 shows that the assigned composition of Au_{~246000}L_{~6280} for the Au–MUTAB nanoparticle agrees with the nanoscaling law, $L = 1.82N^{2/3}$. The linear relation between the points suggests that even at the megadalton mass regime the nanoscaling law is valid and enables the assignment of the composition of nanoparticles.

Our work confirms the role of ligand selection in the design of nanoparticles for applications involving charging in mass spectrometric analysis. Robust patterning is essential for the fabrication of nanoparticle-based devices. Charging of particles is crucial for placing nanoparticles accurately via Coulomb interactions on a charged substrate. In this work, playing with the ligand–gold interface strength (by using thiolates) and permanently charged ligands (trimethylammonium group) leads to high charging in Au–MUTAB gold nanoparticles. Even though the charging efficiency of nanoparticles is enhanced using the MUTAB ligand, it is still challenging to achieve sufficient charging in particles smaller than 20 nm. Future research should focus on ligand selection in nanoparticle design to overcome this limitation. In our proposed electrostatic model, we simplified the gold nanoparticle to a uniformly charged sphere. However, our model is similar to the Rayleigh limit calculations, but instead of equilibrating the electrostatic energy with the surface tension of droplets, here, we equilibrate the electrostatic energy with the total binding energy of charged ligands.

In conclusion, the charging behavior of 20 nm sized gold nanoparticles protected with MUTAB ligands was studied by

using charge detection mass spectrometry (CDMS) interfaced with electrospray ionization. The findings indicate that these nanoparticles can achieve a charging state higher than the theoretical Rayleigh limit for a 20 nm solvent droplet. This charging capability of MUTAB-protected 20 nm particles strongly contrasts with the charging capability of 60 nm citrate-protected AuNPs, which reached only 0.45 times the theoretical limit for similar-sized solvent droplets under similar electrospray conditions. The higher efficiency of MUTAB in enhancing nanoparticle charging may be correlated to the higher ligand binding energy of the gold–sulfur interface as compared with the gold–citrate interface. The estimated binding energies from the CDMS analysis are in fair agreement with the binding energies reported in the literature for thiolate- and citrate-capped gold nanoparticles. One can argue that the charging capability of gas-phase monolayer-protected metal particles generated by electrospray is driven by the ligand binding energy, and therefore, CDMS might be a pertinent probe for determining the ligand binding strength of isolated nanoparticles.

EXPERIMENTAL SECTION

Charge Detection Mass Spectrometry Analysis. MS experiments were performed on the custom-built charge-sensing mass spectrometer coupled with a nanospray source; a 50 μM concentration of Au–MUTAB in water/methanol (50/50 v/v) mixture was used for the measurements. The CDMS instrument was described in detail earlier.^{48,49} The mass spectrometer, operating in the positive mode was equipped with a customized Macrospray (Analytica of Branford)⁴⁸ and Nanospray (nESI) Flex Ion Source (Thermo Fisher Scientific).²⁹ Electrosprayed ions were guided up to the terminal vacuum chamber, which contained the charge detection device (CDD), working in a single-pass mode.^{28,50} The CDD consisted of a conductive tube collinear to the ion beam and connected to a junction field-effect transistor (JFET). The collected signal was amplified by a low-noise charge-sensitive preamplifier (Amptek A250CF CoolFET) and then shaped and differentiated. The signal was recorded with a waveform digitizer card. The data were transferred to a desktop computer, where they were analyzed with an in-house developed program. Calibration in charge was performed using a test capacitor that allowed a known amount of charge to be pulsed onto the pick-up tube. An ionic train device, composed of multipole radiofrequency (RF) ion guides, permitted the transfer of ions (in the optimal 100–100,000 m/z window of transmission) through the capillary interface of the nanoelectrospray ionization source to the charge detection device. The nanospray ionization was customized to fit the entrance of the CDMS instrument. The ion source consisted of a housing with a manual XYZ-manipulator and fittings, a Direct Junction adaptor for online analysis, and a camera setup including one LCD monitor. Electrospray Fused Silica PicoTips (with $\sim 30 \mu\text{m}$ tip inner diameter) were used and changed for each sample analysis.

ASSOCIATED CONTENT

Supporting Information

The Supporting Information is available free of charge at <https://pubs.acs.org/doi/10.1021/acs.jpcllett.5c01075>.

Experimental section, complete information on the CDMS mass and charge plots, TEM images, DLS data,

and isopotential map, HRSEM-EDS elemental analysis, and other data (PDF)

AUTHOR INFORMATION

Corresponding Authors

Rodolphe Antoine – Institut Lumière Matière, University of Lyon, Université Claude Bernard Lyon 1, CNRS, Lyon F-69622, France; Email: rodolphe.antoine@univ-lyon1.fr
Thalappil Pradeep – Department of Chemistry, DST Unit of Nanoscience (DST UNS) and Thematic Unit of Excellence (TUE), Indian Institute of Technology Madras, Chennai 600036, India; International Centre for Clean Water, Chennai, Tamil Nadu 600113, India; orcid.org/0000-0003-3174-534X; Email: pradeep@iitm.ac.in

Authors

B. S. Sooraj – Department of Chemistry, DST Unit of Nanoscience (DST UNS) and Thematic Unit of Excellence (TUE), Indian Institute of Technology Madras, Chennai 600036, India; orcid.org/0000-0002-6963-6491
Sylvain Maclot – Institut Lumière Matière, University of Lyon, Université Claude Bernard Lyon 1, CNRS, Lyon F-69622, France; orcid.org/0000-0001-5587-7182
Anagha Jose – Department of Chemistry, DST Unit of Nanoscience (DST UNS) and Thematic Unit of Excellence (TUE), Indian Institute of Technology Madras, Chennai 600036, India
Clothilde Comby-Zerbino – Institut Lumière Matière, University of Lyon, Université Claude Bernard Lyon 1, CNRS, Lyon F-69622, France
Tessa Reinert – Institut Lumière Matière, University of Lyon, Université Claude Bernard Lyon 1, CNRS, Lyon F-69622, France; orcid.org/0009-0005-7434-8450
Keerthana Unni – Department of Chemistry, DST Unit of Nanoscience (DST UNS) and Thematic Unit of Excellence (TUE), Indian Institute of Technology Madras, Chennai 600036, India

Complete contact information is available at: <https://pubs.acs.org/doi/10.1021/acs.jpcllett.5c01075>

Author Contributions

B.S.S. performed the synthesis, characterization, and other experimental studies. S.M. and T.R. performed the charge detection mass spectrometry studies. A.J. performed the synthesis and characterization studies of nanoparticles. C.C.Z. performed the DLS measurements. K.U. performed the elemental analysis of the samples. B.S.S. wrote the first draft with inputs from R.A. T.P. and R.A. conceptualized the work, discussed the results, and edited the final version of the manuscript. All authors have approved the final version of the manuscript.

Notes

The authors declare no competing financial interest.

ACKNOWLEDGMENTS

B.S.S. thanks the Council of Scientific & Industrial Research (CSIR) for the Shyama Prasad Mukherjee (SPM) fellowship. S.M. is grateful for the postdoc fellowship of the Horizon 2020 Research and Innovation program under grant #964553 (project ARIADNE-Vibe). A.J. thanks the Ministry of Human Resources and Development (MHRD) for the Prime Minister's Research Fellowship (PMRF). K.U. thanks the

University Grants Commission (UGC) for the research fellowship. T.P. thanks the Science and Engineering Research Board (SERB), India, for funding through the research grant, SPR/2021/000439 and through a JC Bose Fellowship. T.P. also acknowledges funding from the Centre of Excellence on Molecular Materials and Functions under the Institution of Eminence scheme of IIT Madras. We acknowledge Indo-French Centre for the Promotion of Advanced Research (IFCPAR/CEFIPRA) for funding through the workshop on metal nanoclusters and their self-assembly initiating this collaborative work. R.A. thanks French National Centre for Scientific Research (CNRS) for funding through International Emerging Actions between France and India. R.A. acknowledges Agence Nationale de la Recherche (projects MANBAMM, ANR-21-CE29-0020, nanoGOLD, ANR-22-CE29-0022 and MOONSTONE, ANR-22-CE42-0031), the European Horizon 2020 research and innovation program's projects #964553 (ARIADNE-Vibe) and HORIZON-EIC-2022-PATHFINDEROPEN-01 #101099058 (Virusong) for support. The authors would like to thank Fabien Rossetti (iLM) for the DLS measurements.

DEDICATION

Dedicated to Prof. R. Graham Cooks on the occasion of his 84th birthday.

REFERENCES

- (1) Barbalinardo, M.; Ori, G.; Lungaro, L.; Caio, G.; Migliori, A.; Gentili, D. Direct Cationization of Citrate-Coated Gold and Silver Nanoparticles. *J. Phys. Chem. C* **2024**, *128* (38), 16220–16226.
- (2) Heuer-Jungemann, A.; Feliu, N.; Bakaimi, I.; Hamaly, M.; Alkilany, A.; Chakraborty, I.; Masood, A.; Casula, M. F.; Kostopoulou, A.; Oh, E.; Susumu, K.; Stewart, M. H.; Medintz, I. L.; Stratakis, E.; Parak, W. J.; Kanaras, A. G. The Role of Ligands in the Chemical Synthesis and Applications of Inorganic Nanoparticles. *Chem. Rev.* **2019**, *119* (8), 4819–4880.
- (3) Daniel, M.-C.; Astruc, D. Gold Nanoparticles: Assembly, Supramolecular Chemistry, Quantum-Size-Related Properties, and Applications toward Biology, Catalysis, and Nanotechnology. *Chem. Rev.* **2004**, *104* (1), 293–346.
- (4) Ishida, Y.; Suzuki, J.; Akita, I.; Yonezawa, T. Ultrarapid Cationization of Gold Nanoparticles via a Single-Step Ligand Exchange Reaction. *Langmuir* **2018**, *34* (36), 10668–10672.
- (5) Tsunoyama, H.; Sakurai, H.; Ichikuni, N.; Negishi, Y.; Tsukuda, T. Colloidal Gold Nanoparticles as Catalyst for Carbon-Carbon Bond Formation: Application to Aerobic Homocoupling of Phenylboronic Acid in Water. *Langmuir* **2004**, *20* (26), 11293–11296.
- (6) Alloway, D. M.; Graham, A. L.; Yang, X.; Mudalige, A.; Colorado, R.; Wysocki, V. H.; Pemberton, J. E.; Lee, T. R.; Wysocki, R. J.; Armstrong, N. R. Tuning the Effective Work Function of Gold and Silver Using ω -Functionalized Alkanethiols: Varying Surface Composition through Dilution and Choice of Terminal Groups. *J. Phys. Chem. C* **2009**, *113* (47), 20328–20334.
- (7) Baer, D. R.; Engelhard, M. H.; Johnson, G. E.; Laskin, J.; Lai, J.; Mueller, K.; Munusamy, P.; Thevuthasan, S.; Wang, H.; Washton, N.; Elder, A.; Baisch, B. L.; Karakoti, A.; Kuchibhatla, S. V. N. T.; Moon, D. Surface Characterization of Nanomaterials and Nanoparticles: Important Needs and Challenging Opportunities. *J. Vac. Sci. Technol. A* **2013**, *31* (5), 50820.
- (8) Jose, A.; Walker, J. N.; Khatun, M.; Malola, S.; Sooraj, B. S.; Häkkinen, H.; Brodbelt, J. S.; Pradeep, T. Ultraviolet Photoactivation Perturbs the Metal-Ligand Interface of Atomically Precise Nanoclusters. *Chem. Commun.* **2025**, *61* (35), 6482–6485.
- (9) Bustos, A. R. M.; Encinar, J. R.; Sanz-Medel, A. Mass Spectrometry for the Characterisation of Nanoparticles. *Anal. Bioanal. Chem.* **2013**, *405* (17), 5637–5643.
- (10) Comby-Zerbino, C.; Dagany, X.; Chirot, F.; Dugourd, P.; Antoine, R. The Emergence of Mass Spectrometry for Characterizing Nanomaterials. Atomically Precise Nanoclusters and Beyond. *Mater. Adv.* **2021**, *2* (15), 4896–4913.
- (11) Lai, S.-H.; Maclot, S.; Antoine, R.; Masselon, C. D. Advances in Single Particle Mass Analysis. *Mass Spectrom. Rev.* **2024**, 1–20.
- (12) Jarrold, M. F. Single-Ion Mass Spectrometry for Heterogeneous and High Molecular Weight Samples. *J. Am. Chem. Soc.* **2024**, *146* (9), 5749–5758.
- (13) Doussineau, T.; Désert, A.; Lambert, O.; Taveau, J. C.; Lansalot, M.; Dugourd, P.; Bourgeat-Lami, E.; Ravaine, S.; Duguet, E.; Antoine, R. Charge Detection Mass Spectrometry for the Characterization of Mass and Surface Area of Composite Nanoparticles. *J. Phys. Chem. C* **2015**, *119* (20), 10844–10849.
- (14) Keifer, D. Z.; Shinholt, D. L.; Jarrold, M. F. Charge Detection Mass Spectrometry with Almost Perfect Charge Accuracy. *Anal. Chem.* **2015**, *87* (20), 10330–10337.
- (15) Kafader, J. O.; Melani, R. D.; Durbin, K. R.; Ikwuagwu, B.; Early, B. P.; Fellers, R. T.; Beu, S. C.; Zabrouskov, V.; Makarov, A. A.; Maze, J. T.; Shinholt, D. L.; Yip, P. F.; Tullman-Ercek, D.; Senko, M. W.; Compton, P. D.; Kelleher, N. L. Multiplexed Mass Spectrometry of Individual Ions Improves Measurement of Proteoforms and Their Complexes. *Nat. Methods* **2020**, *17* (4), 391–394.
- (16) Doussineau, T.; Bao, C. Y.; Antoine, R.; Dugourd, P.; Zhang, W.; D'Agosto, F.; Charleux, B. Direct Molar Mass Determination of Self-Assembled Amphiphilic Block Copolymer Nanoobjects Using Electrospray-Charge Detection Mass Spectrometry. *ACS Macro Lett.* **2012**, *1* (3), 414–417.
- (17) Loumaigne, M.; Midelet, C.; Doussineau, T.; Dugourd, P.; Antoine, R.; Stamboul, M.; Débarre, A.; Werts, M. H. V. Optical Extinction and Scattering Cross Sections of Plasmonic Nanoparticle Dimers in Aqueous Suspension. *Nanoscale* **2016**, *8* (12), 6555–6570.
- (18) Harper, C. C.; Miller, Z. M.; McPartlan, M. S.; Jordan, J. S.; Pedder, R. E.; Williams, E. R. Accurate Sizing of Nanoparticles Using a High-Throughput Charge Detection Mass Spectrometer without Energy Selection. *ACS Nano* **2023**, *17* (8), 7765–7774.
- (19) Harper, C. C.; Jordan, J. S.; Papanu, S.; Williams, E. R. Characterization of Mass, Diameter, Density, and Surface Properties of Colloidal Nanoparticles Enabled by Charge Detection Mass Spectrometry. *ACS Nano* **2024**, *18* (27), 17806–17814.
- (20) Miller, L. M.; Young, T. W.; Wang, Y.; Draper, B. E.; Ye, X.; Jacobson, S. C.; Jarrold, M. F. Complementary Nanoparticle Characterization by Resistive-Pulse Sensing, Electron Microscopy, and Charge Detection Mass Spectrometry. *Anal. Chem.* **2024**, *96* (35), 14239–14247.
- (21) Doussineau, T.; Santacreu, M.; Antoine, R.; Dugourd, P.; Zhang, W.; Chaduc, I.; Lansalot, M.; D'Agosto, F.; Charleux, B. The Charging of Micellar Nanoparticles in Electrospray Ionization. *ChemPhysChem* **2013**, *14* (3), 603–609.
- (22) Ouadah, N.; Doussineau, T.; Hamada, T.; Dugourd, P.; Bordes, C.; Antoine, R. Correlation between the Charge of Polymer Particles in Solution and in the Gas Phase Investigated by Zeta-Potential Measurements and Electrospray Ionization Mass Spectrometry. *Langmuir* **2013**, *29* (46), 14074–14081.
- (23) Suh, J.; Han, B.; Okuyama, K.; Choi, M. Highly Charging of Nanoparticles through Electrospray of Nanoparticle Suspension. *J. Colloid Interface Sci.* **2005**, *287* (1), 135–140.
- (24) Konermann, L. A Simple Model for the Disintegration of Highly Charged Solvent Droplets during Electrospray Ionization. *J. Am. Soc. Mass Spectrom.* **2009**, *20* (3), 496–506.
- (25) Konermann, L.; Ahadi, E.; Rodriguez, A. D.; Vahidi, S. Unraveling the Mechanism of Electrospray Ionization. *Anal. Chem.* **2013**, *85* (1), 2–9.
- (26) Going, C. C.; Xia, Z.; Williams, E. R. New Supercharging Reagents Produce Highly Charged Protein Ions in Native Mass Spectrometry. *Analyst* **2015**, *140* (21), 7184–7194.
- (27) Miladinović, S. M.; Fornelli, L.; Lu, Y.; Piech, K. M.; Girault, H. H.; Tsybin, Y. O. In-Spray Supercharging of Peptides and Proteins in

- Electrospray Ionization Mass Spectrometry. *Anal. Chem.* **2012**, *84* (11), 4647–4651.
- (28) Antoine, R. Weighing Synthetic Polymers of Ultra-High Molar Mass and Polymeric Nanomaterials: What Can We Learn from Charge Detection Mass Spectrometry? *Rapid Commun. Mass Spectrom.* **2020**, *34* (S2), No. e8539.
- (29) Tsirkou, A.; Kaczorowski, F.; Verduran, M.; Raffoul, R.; Pansieri, J.; Quadrio, I.; Chauveau, F.; Antoine, R. Charge Detection Mass Spectrometry on Human-Amplified Fibrils from Different Synucleinopathies. *Chem. Commun.* **2022**, *58* (51), 7192–7195.
- (30) Shen, C.; Xue, Y.; Li, Y.; Wei, M.; Wen, M.; Zhang, L.; Shang, L. Kinetically Regulated One-Pot Synthesis of Cationic Gold Nanoparticles and Their Size-Dependent Antibacterial Mechanism. *J. Mater. Sci. Technol.* **2023**, *162*, 145–156.
- (31) Rayleigh, L. On the Equilibrium of Liquid Conducting Masses Charged with Electricity. *Philos. Mag.* **1882**, *14* (87), 184–186.
- (32) Elliott, A. G.; Merenbloom, S. I.; Chakrabarty, S.; Williams, E. R. Single Particle Analyzer of Mass: A Charge Detection Mass Spectrometer with a Multi-Detector Electrostatic Ion Trap. *Int. J. Mass Spectrom.* **2017**, *414*, 45–55.
- (33) Nuzzo, R. G.; Zegarski, B. R.; Dubois, L. H. Fundamental Studies of the Chemisorption of Organosulfur Compounds on Gold (111). Implications for Molecular Self-Assembly on Gold Surfaces. *J. Am. Chem. Soc.* **1987**, *109* (3), 733–740.
- (34) Chen, F.; Li, X.; Hihath, J.; Huang, Z.; Tao, N. Effect of Anchoring Groups on Single-Molecule Conductance: Comparative Study of Thiol-, Amine-, and Carboxylic-Acid-Terminated Molecules. *J. Am. Chem. Soc.* **2006**, *128* (49), 15874–15881.
- (35) Hinterwirth, H.; Kappel, S.; Waitz, T.; Prohaska, T.; Lindner, W.; Lämmerhofer, M. Quantifying Thiol Ligand Density of Self-Assembled Monolayers on Gold Nanoparticles by Inductively Coupled Plasma-Mass Spectrometry. *ACS Nano* **2013**, *7* (2), 1129–1136.
- (36) Franco-Ulloa, S.; Tatulli, G.; Bore, S. L.; Moglianetti, M.; Pompa, P. P.; Cascella, M.; De Vivo, M. Dispersion State Phase Diagram of Citrate-Coated Metallic Nanoparticles in Saline Solutions. *Nat. Commun.* **2020**, *11* (1), 5422.
- (37) Chong, G.; Hernandez, R. Adsorption Dynamics and Structure of Polycations on Citrate-Coated Gold Nanoparticles. *J. Phys. Chem. C* **2018**, *122* (34), 19962–19969.
- (38) Lin, Y.; Pan, G. B.; Su, G. J.; Fang, X. H.; Wan, L. J.; Bai, C. L. Study of Citrate Adsorbed on the Au(111) Surface by Scanning Probe Microscopy. *Langmuir* **2003**, *19* (24), 10000–10003.
- (39) Scanlon, M. D.; Peljo, P.; Méndez, M. A.; Smirnov, E.; Girault, H. H. Charging and Discharging at the Nanoscale: Fermi Level Equilibration of Metallic Nanoparticles. *Chem. Sci.* **2015**, *6* (5), 2705–2720.
- (40) Henglein, A. Physicochemical Properties of Small Metal Particles in Solution: “Microelectrode” Reactions, Chemisorption, Composite Metal Particles, and the Atom-to-Metal Transition. *J. Phys. Chem.* **1993**, *97* (21), 5457–5471.
- (41) Dass, A. Nano-Scaling Law: Geometric Foundation of Thiolated Gold Nanomolecules. *Nanoscale* **2012**, *4* (7), 2260–2263.
- (42) Otto, H. H. Ratio of In-Sphere Volume to Polyhedron Volume of the Great Pyramid Compared to Selected Convex Polyhedral Solids. *J. Appl. Math. Phys.* **2021**, *09* (01), 41–56.
- (43) Boulanger, N.; Buisseret, F.; Dierick, F.; White, O. The Two-Thirds Power Law Derived from an Higher-Derivative Action. *Physics* **2024**, *6* (4), 1251–1263.
- (44) Vergara, S.; Santiago, U.; Kumara, C.; Alducin, D.; Whetten, R. L.; Jose Yacaman, M.; Dass, A.; Ponce, A. Synthesis, Mass Spectrometry, and Atomic Structural Analysis of Au_{~2000}(SR)_{~290} Nanoparticles. *J. Phys. Chem. C* **2018**, *122* (46), 26733–26738.
- (45) Kumara, C.; Hoque, M. M.; Zuo, X.; Cullen, D. A.; Whetten, R. L.; Dass, A. Isolation of a 300 KDa, Au_{~1400} Gold Compound, the Standard 3.6 Nm Capstone to a Series of Plasmonic Nanocrystals Protected by Aliphatic-like Thiolates. *J. Phys. Chem. Lett.* **2018**, *9* (23), 6825–6832.
- (46) Kumara, C.; Zuo, X.; Cullen, D. A.; Dass, A. Faradaurate-940: Synthesis, Mass Spectrometry, Electron Microscopy, High-Energy X-Ray Diffraction, and X-Ray Scattering Study of Au_{~940 ± 20}(SR)_{~160 ± 4} Nanocrystals. *ACS Nano* **2014**, *8* (6), 6431–6439.
- (47) Kumara, C.; Zuo, X.; Ilavsky, J.; Chapman, K. W.; Cullen, D. A.; Dass, A. Super-Stable, Highly Monodisperse Plasmonic Faradaurate-500 Nanocrystals with 500 Gold Atoms: Au_{~500}(SR)_{~120}. *J. Am. Chem. Soc.* **2014**, *136* (20), 7410–7417.
- (48) Doussineau, T.; Kerleroux, M.; Dagany, X.; Clavier, C.; Barbaire, M.; Maurelli, J.; Antoine, R.; Dugourd, P. Charging Megadalton Poly(Ethylene Oxide)s by Electrospray Ionization. A Charge Detection Mass Spectrometry Study. *Rapid Commun. Mass Spectrom.* **2011**, *25* (5), 617–623.
- (49) Doussineau, T.; Yu Bao, C.; Clavier, C.; Dagany, X.; Kerleroux, M.; Antoine, R.; Dugourd, P. Infrared Multiphoton Dissociation Tandem Charge Detection-Mass Spectrometry of Single Megadalton Electrospayed Ions. *Rev. Sci. Instrum.* **2011**, *82* (8), No. 084104.
- (50) Keifer, D. Z.; Pierson, E. E.; Jarrold, M. F. Charge Detection Mass Spectrometry: Weighing Heavier Things. *Analyst* **2017**, *142* (10), 1654–1671.